Terahertz radiation and second-harmonic generation from InAs: Bulk versus surface electric-field-induced contributions

Matthew Reid, Igor V. Cravetchi, and Robert Fedosejevs
Department of Electrical and Computer Engineering, University of Alberta, Edmonton, Alberta, Canada T6G 2V4
(Received 27 February 2005; published 5 July 2005)

Polarized second-harmonic generation and terahertz radiation in reflection from (100), (110), and (111) faces of *n*-type InAs crystals are investigated as a function of the sample azimuthal orientation under excitation from femtosecond Ti:sapphire laser pulses. The expressions describing the second-order response (optical second-harmonic generation and optical rectification) in reflection from zinc-blende crystals, such as InAs, are calculated taking into account the bulk electric-dipole contribution and the first-order surface electric-field-induced contribution. It is shown that the two contributions can be separated based on rotation symmetry considerations. Moreover, a direct comparison of the second-harmonic generation and terahertz radiation emission indicates that the observed dominant surface electric-field-induced optical rectification component may be attributed to the large free-carrier contribution to the third-order susceptibility in InAs.

DOI: 10.1103/PhysRevB.72.035201 PACS number(s): 42.65.Re, 42.65.Ky

I. INTRODUCTION

The generation of pulsed radiation in the terahertz (THz) frequency band is of significant interest at the present time due to a growing number of applications such as imaging,[1–3] illicit-drug detection,[4] and biomedical applications.[3,5] The three methods traditionally used to generate pulsed THz radiation are (i) transient current generation at semiconductor surfaces,[6] (ii) emission from a photoconductive switch,[7] and (iii) nonlinear optical interactions.[8,9]

The generation of terahertz radiation from semiconductor surfaces has attracted much attention since initial reports of high conversion efficiencies, using InAs in a magnetic field.[10] Since this time, InAs surface emission has proven to be a relatively bright source of pulsed THz radiation, especially under the influence of an external magnetic field.[11–13] However, it suffers from a lower conversion efficiency in comparison to photoconductive emitters.[14]

The emission of THz radiation from semiconductor surfaces is very complex due to multiple competing mechanisms leading to the radiation. Contributions from photocarrier acceleration in the depletion field,[6,15] photocarrier diffusion,[16] and optical rectification[17–19] have all been reported. The relative magnitudes of radiation resulting from the various processes is strongly dependent on excitation fluence.[20] In order to fully understand the limitations on the generation of THz radiation, it is important to clearly differentiate all of the mechanisms leading to the emission.

In the present paper, the azimuthal symmetry of THz radiation from InAs due to an effective second-order nonlinearity is studied in detail. In order to clearly operate in a regime where the nonlinear optical response of InAs dominates the THz emission process, the characteristics of the THz emission are examined at high excitation fluences ($1-2$ mJ/cm^2).[21] The expressions for the azimuthal-angle dependencies of the bulk electric-dipole and surface electric-field-induced (SEFI) contributions are calculated and compared with the results of optical second-harmonic generation (SHG) and optical rectification (OR) from the InAs samples. It is shown that while SHG is dominated by the bulk electric-dipole contribution, the terahertz emission is dominated by the surface electric-field-induced contribution.

II. BACKGROUND

In the electric-dipole approximation, the second-order polarization responsible for the nonlinear optical processes of optical rectification and second-harmonic generation is given by[22]

$$\mathbf{P}_i^{(2)}(\Omega) = \chi_{ijk}^{(2)\mathrm{eff}}(\Omega; -\omega, \omega) : \mathbf{E}_j(-\omega)\mathbf{E}_k(\omega), \tag{1}$$

where the effective second-order susceptibility, $\chi_{ijk}^{(2)\mathrm{eff}}$, can have contributions from many sources such as bulk, $\chi_{ijk}^{(2)\mathrm{bulk}}$, surface, $\chi_{ijk}^{(2)\mathrm{surf}}$ and effective second-order processes such as electric-field-induced optical rectification. In the latter case, a dc field in combination with higher order nonlinearities produces an effective second-order process. For a dc field resulting from the surface-electric field (SEF), we consider only the term of first-order in the expansion (see Sec. II B), giving $\chi_{ijk}^{(2)\mathrm{SEF}} = 3\chi_{ijkz}^{(3)} E_z^{\mathrm{surf}}$, where E_z^{surf} is the SEF. In the present report, we consider the effective nonlinear susceptibility to be[23]

$$\chi_{ijk}^{(2)\mathrm{eff}} = \chi_{ijk}^{(2)\mathrm{bulk}} + 3\chi_{ijkz}^{(3)} E_z^{\mathrm{surf}}, \tag{2}$$

where $\chi_{ijk}^{(2)\mathrm{bulk}}$ is the second-order susceptibility tensor determined by the symmetry properties of the bulk material (the thickness of the contributing material layer is restricted by the absorption depth of the pump radiation or escape depth of the harmonic radiation) and $\chi_{ijkz}^{(3)}$ is the third-order susceptibility tensor that specifies the symmetry properties of radiation from the near-surface region which is under the influence of a surface electric field. The intrinsic surface contribution is assumed to be negligible in noncentrosymmetric crystals such as InAs and is not included.[22,24,25]

Substituting Eq. (2) into Eq. (1) it is seen that in general the nonlinear response from noncentrosymmetric material is a result of interference between intrinsic bulk contribution

 ©2005 The American Physical Society

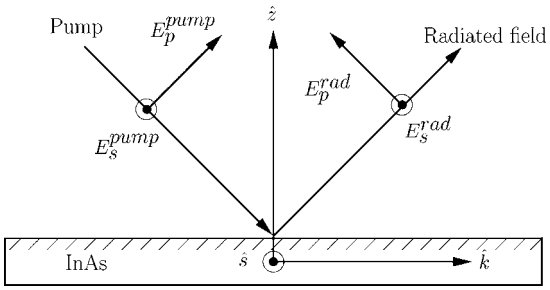

FIG. 1. Geometry for polarizations and surface orientation of InAs wafers used in the calculations. The pump beam is linearly polarized and the *s*- and *p*-polarized radiated fields are examined.

and SEF induced contribution. As is shown below, the analysis based only on symmetry considerations makes it possible to differentiate between these two main contributions for the processes of radiation from optical rectification or second-harmonic generation from some standard crystallographic faces of InAs.

In this section we will outline the expected bulk second-order nonlinear response of zinc-blende crystals with $\bar{4}3m$ symmetry in a reflection geometry under crystal rotation. The calculations will be performed for the three crystallographic faces (100), (110), and (111). The polarization and emission characteristics of surface-field induced optical rectification are calculated next.

A. Bulk nonlinear optical response

Crystalline InAs has a zinc-blende structure, possessing $\bar{4}3m$ symmetry. The second-order susceptibility tensor therefore has only six nonvanishing tensor elements, all of which are equal: $\chi^{(2)}_{xyz}=\chi^{(2)}_{xzy}=\chi^{(2)}_{yzx}=\chi^{(2)}_{yxz}=\chi^{(2)}_{zxy}=\chi^{(2)}_{zyx}$.[22] In order to determine the far-infrared polarization at frequency Ω of the InAs lattice that results from an optical field at frequency ω we compute

$$\mathbf{P}^{(2)}(\Omega)=\chi^{(2)\text{bulk}}(\Omega;-\omega,\omega):\mathbf{E}_{\text{opt}}(-\omega)\mathbf{E}_{\text{opt}}(\omega). \quad (3)$$

It should be noted that the calculation that follows is sufficient to describe the process of second-harmonic generation, as the only difference is that the polarization of the lattice occurs at the sum frequency ($\omega+\omega=2\omega$), whereas the far-infrared generation occurs at the difference frequency ($\omega-\omega=\Omega\sim 0$). In addition, the calculation is performed only for the bulk electric-dipole contribution, and higher-order multipoles are not included.

As the second-order polarization depends on the orientation of $\mathbf{E}_{\text{opt}}(\omega)$ with respect to the crystal axes, it is useful to transform the coordinate system to the beam coordinate system.[24] Defining the $(\hat{s},\hat{k},\hat{z})$ coordinate system, such that the $\hat{s}$ axis is in the surface of the crystal and parallel to an input *s*-polarized pump beam, $\hat{z}$ is normal to the crystal surface and $\hat{k}=\hat{z}\times\hat{s}$ (see Fig. 1), we can define a rotation matrix, R^{xtal}, from crystallographic coordinates to the beam coordinate system for each of the crystal faces: (111), (110), and (100) studied in the present report. For each of the crystal faces, the crystallographic coordinate system is rotated such that the $\hat{z}$ axis is parallel to the [111], [110], and [100] crystallographic axis, respectively.

For the bulk contribution to the radiated field, we are interested in the dependence of the THz field amplitude under crystal rotation about the surface normal. We define another rotation matrix, $R^{\text{rot}}(\phi)$, that defines the angle of rotation of the crystal about its surface normal. For the (111) crystal face, ϕ is defined as the angle between the $\hat{k}$ axis and the crystal $[\bar{2}11]$ axis. For the (110) face, ϕ is defined as the angle between the $\hat{k}$ axis and the crystal $[1\bar{1}0]$ axis. For the (100) crystal face, ϕ is defined as the angle between $\hat{k}$ and the crystal $[01\bar{1}]$ axis. From this, we can compute the susceptibility tensor in the beam coordinate system as a function of ϕ by applying the tensor transformation properties of a third rank tensor, and using the total transformation $R^{\text{tot}}=R^{\text{rot}}R^{\text{xtal}}$:

$$\chi^{(2)}_{ijk}(\phi)=\sum_{lmn}(R^{\text{tot}}_{il}R^{\text{tot}}_{jm}R^{\text{tot}}_{kn}\chi^{(2)}_{lmn}). \quad (4)$$

Substituting the susceptibility from Eq. (4) in Eq. (3), the independent lattice polarizations can be found. In turn, the *s*-polarized and *p*-polarized radiation resulting from the lattice polarization is readily obtained.[26] The results are tabulated for the different polarization combinations, listed as $E_{\text{in,out}}$, in Table I. The coefficients f_s, f_c, t_s, t_p, A_s, A_p, F_s, and F_c are as defined in Ref. 27, and depend on the angle of incidence and the linear optical properties of the material. L_{eff} is the effective depth of the medium from which the medium polarization contributes to SHG and d_{14} is the only nonvanishing tensor element in contracted notation.

B. Surface nonlinear optical response

The third-order susceptibility tensor for zinc-blende crystals with $\bar{4}3m$ symmetry, $\chi^{(3)}_{ijkl}$, has only 21 nonzero elements, 4 of which are unique: $\chi^{(3)}_{iijj}$, $\chi^{(3)}_{ijij}$, $\chi^{(3)}_{ijji}$, and $\chi^{(3)}_{iiii}$.[28] This can lead to an effective second-order nonlinearity, $\chi^{(2)\text{eff}}_{ijk}$, if a dc field is involved. In the present case, we consider a surface field in the $\hat{z}$ direction normal to the surface, resulting from the space-charge layer at the InAs/native oxide interface. Following Germer *et al.*,[23] the effective nonlinear susceptibility, $\chi^{(2)\text{eff}}_{ijk}$ in the electric-dipole approximation, can be expanded in terms of the surface electric-field, E_z^{surf}, to first-order:

$$\chi^{(2)\text{eff}}_{ijk}=\chi^{(2)}_{ijk}(\Omega;-\omega,\omega)+3\chi^{(3)}_{ijkz}(\Omega;-\omega,\omega,0)(E_z^{\text{surf}}). \quad (5)$$

It is assumed that the first-order term in the surface electric field dominates and that higher order contributions will be small. Considering only the term of first-order in the surface field [i.e., the second term on the left-hand side (LHS) of Eq. (5)], we can write the effective surface electric field (SEF) induced second-order response of the system, $\chi^{(2)\text{SEF}}_{ijk}$ as

$$\chi^{(2)\text{SEF}}_{ijk}=3\chi^{(3)}_{ijkz}(\Omega;-\omega,\omega,0)E_z^{\text{surf}}. \quad (6)$$

To properly examine the effective second-order surface response, we transform the susceptibility tensor to beam co-

TABLE I. THz field strengths for different polarization combinations. Combinations are listed as $E_{\text{in,out}}$.

Bulk dipole nonlinear response

(111) **crystal face**

$$E_{p,p}^{\text{THz}} = \frac{1}{\sqrt{3}} A_p L_{\text{eff}} \Omega d_{14} t_p^2 E_p^2 [(2F_s f_s^2 - F_s f_c^2 + 2F_c f_s f_c) - (\sqrt{2} F_c f_c^2)\cos(3\phi)]$$

$$E_{p,s}^{\text{THz}} = \sqrt{\frac{2}{3}} A_s L_{\text{eff}} \Omega d_{14} t_p^2 f_c^2 E_p^2 \sin(3\phi)$$

(100) **crystal face**

$$E_{p,p}^{\text{THz}} = A_p L_{\text{eff}} \Omega d_{14} t_p^2 E_p^2 [2F_c f_s f_c - F_s f_c^2] \cos(2\phi)$$

$$E_{p,s}^{\text{THz}} = -2A_s L_{\text{eff}} \Omega d_{14} t_p^2 E_p^2 f_s f_c \sin(2\phi)$$

(110) **crystal face**

$$E_{p,p}^{\text{THz}} = A_p L_{\text{eff}} \Omega d_{14} t_p^2 E_p^2 \left[\left(2F_s f_s f_c - F_c f_s^2 - \frac{3}{4} F_c f_c^2 \right) \sin(\phi) + \frac{3}{4} F_c f_c^2 \sin(3\phi) \right]$$

$$E_{p,s}^{\text{THz}} = A_s L_{\text{eff}} \Omega d_{14} t_p^2 E_p^2 \left[\left(\frac{1}{4} f_c^2 - f_s^2 \right) \cos(\phi) + \frac{3}{4} f_c^2 \cos(3\phi) \right]$$

ordinates (as done in Sec. II A), so that the surface field lies along the $\hat{z}$ axis (see Fig. 1). To illustrate this, we consider the (111) crystal face, where the transformation matrix is given by Eq. (7).

$$R_{\text{rot}}^{(111)} = \begin{pmatrix} \sqrt{\frac{2}{3}} & -\frac{1}{\sqrt{6}} & -\frac{1}{\sqrt{6}} \\ 0 & \frac{1}{\sqrt{2}} & -\frac{1}{\sqrt{2}} \\ \frac{1}{\sqrt{3}} & \frac{1}{\sqrt{3}} & \frac{1}{\sqrt{3}} \end{pmatrix}. \tag{7}$$

Using the transformation properties of a fourth rank tensor, $\chi_{\alpha\beta\gamma\delta}^{\text{rot}} = \Sigma_{lmno} R_{\alpha l}^{\text{rot}} R_{\beta m}^{\text{rot}} R_{\gamma n}^{\text{rot}} R_{\delta o}^{\text{rot}} \chi_{lmno}^{(3)}$, contracted with the surface field, we expect the form of the effective SEF induced second-order tensor to be

$$\chi_{\alpha\beta\gamma}^{(2)\text{SEF}} = 3E_z^{\text{surf}} \sum_{lmno} R_{\alpha l}^{\text{rot}} R_{\beta m}^{\text{rot}} R_{\gamma n}^{\text{rot}} R_{zo}^{\text{rot}} \chi_{lmno}^{(3)}. \tag{8}$$

Applying the rotation matrix, Eq. (7), and evaluating each independent tensor element (18 in total), using Eq. (8), we obtain for the (111) crystal face the effective SEF induced second-order susceptibility:

$$(\chi_{xyz}^{(2)\text{SEF}})_{(111)} = \begin{pmatrix} \partial_{11} & -\partial_{11} & 0 & 0 & \partial_{15} & 0 \\ 0 & 0 & 0 & \partial_{15} & 0 & -\partial_{11} \\ \partial_{31} & \partial_{31} & \partial_{33} & 0 & 0 & 0 \end{pmatrix}, \tag{9}$$

where we have

$$\partial_{11} = \frac{E_z^{\text{surf}}}{\sqrt{2}} (-\chi_{iijj}^{(3)} - \chi_{ijij}^{(3)} - \chi_{ijji}^{(3)} + \chi_{iiii}^{(3)}),$$

$$\partial_{15} = E_z^{\text{surf}} (2\chi_{iijj}^{(3)} - \chi_{ijij}^{(3)} - \chi_{ijji}^{(3)} + \chi_{iiii}^{(3)}),$$

$$\partial_{31} = E_z^{\text{surf}} (-\chi_{iijj}^{(3)} - \chi_{ijij}^{(3)} + 2\chi_{ijji}^{(3)} + \chi_{iiii}^{(3)}),$$

$$\partial_{33} = E_z^{\text{surf}} (2\chi_{iijj}^{(3)} + 2\chi_{ijij}^{(3)} + 2\chi_{ijji}^{(3)} + \chi_{iiii}^{(3)}). \tag{10}$$

It should be noted that, in general, the only symmetry conditions that can be applied in the present case, due to above-band-gap excitation, and without knowing all the system resonances, is that of intrinsic permutation symmetry.[22] Given that we have optical frequency ω, far-infrared frequency Ω, and the SEF at zero frequency $[\chi_{ijkl}^{(3)}(\Omega;\omega, -\omega, 0)]$, the intrinsic permutation symmetry allows interchanging the second and third indices, which will reduce the independent susceptibility elements to 3: $\chi_{iiii}^{(3)}$, $\chi_{ijij}^{(3)} (= \chi_{iijj}^{(3)})$ and $\chi_{ijji}^{(3)}$. If the far-infrared frequency, $\Omega \sim 0$, is approximated as a dc field, and overall permutation symmetry holds, the number of independent susceptibility elements will be 2: $\chi_{iiii}^{(3)}$ and $\chi_{ijij}^{(3)} (= \chi_{iijj}^{(3)} = \chi_{ijji}^{(3)})$.

TABLE II. THz field strengths for different polarization combinations. Combinations are listed as $E_{\text{in,out}}$.

Surface electric field induced nonlinear response
(111) **crystal face**
$E_{p,p}^{\text{THz}} = A_p L_{\text{eff}} \Omega E_p^2 t_p^2 [F_s f_c^2 \partial_{31} + F_s f_s^2 \partial_{33} - 2F_c f_s f_c \partial_{15}] - A_p L_{\text{eff}} \Omega E_p^2 t_p^2 [F_c f_s^2 \partial_{11}] \cos(3\phi)$
$E_{p,s}^{\text{THz}} = A_s L_{\text{eff}} \Omega E_p^2 t_p^2 f_c^2 \partial_{11} \sin(3\phi)$
(100) **crystal face**
$E_{p,p}^{\text{THz}} = A_p L_{\text{eff}} \Omega E_p^2 t_p^2 [-2\partial_{15} F_c f_s f_c + F_s f_c^2 \partial_{31} + F_s f_s^2 \partial_{33}]$
$E_{p,s}^{\text{THz}} = 0$
(110) **crystal face**
$E_{p,p}^{\text{THz}} = A_p L_{\text{eff}} \Omega E_p^2 t_p^2 [F_s f_s^2 \partial_{33} + F_s f_c^2 \partial_{32} - 2F_s f_c f_s \partial_{24}] + A_p L_{\text{eff}} \Omega E_p^2 t_p^2 \left[\frac{1}{2} F_s f_c^2 (\partial_{31} - \partial_{32}) - F_s f_s f_c (\partial_{15} - \partial_{24}) \right]$
$+ A_p L_{\text{eff}} \Omega E_p^2 t_p^2 \left[\frac{1}{2} F_s f_c^2 (\partial_{31} - \partial_{32}) - F_s f_c f_s (\partial_{15} - \partial_{24}) \right] \cos(2\phi)$
$E_{p,s}^{\text{THz}} = A_s L_{\text{eff}} \Omega E_p^2 t_p^2 f_s f_c (\partial_{15} - \partial_{24}) \sin(2\phi)$

Similarly, applying the appropriate transformation matrices to the (110) and (100) crystal faces, we obtain the effective SEF induced second-order susceptibility as

$$(\chi_{xyz}^{(2)\text{SEF}})_{(110)} = \begin{pmatrix} 0 & 0 & 0 & 0 & \partial_{15} & 0 \\ 0 & 0 & 0 & \partial_{24} & 0 & 0 \\ \partial_{31} & \partial_{32} & \partial_{33} & 0 & 0 & 0 \end{pmatrix}, \quad (11)$$

where we have

$$\partial_{15} = \frac{3E_z^{\text{surf}}}{2} (\chi_{iijj}^{(3)} - \chi_{ijij}^{(3)} - \chi_{ijji}^{(3)} + \chi_{iiii}^{(3)}),$$

$$\partial_{24} = 3E_z^{\text{surf}} \chi_{iijj}^{(3)},$$

$$\partial_{31} = \frac{3E_z^{\text{surf}}}{2} (-\chi_{iijj}^{(3)} - \chi_{ijij}^{(3)} + \chi_{ijji}^{(3)} + \chi_{iiii}^{(3)}),$$

$$\partial_{32} = 3E_z^{\text{surf}} \chi_{ijji}^{(3)},$$

$$\partial_{33} = \frac{3E_z^{\text{surf}}}{2} (\chi_{iijj}^{(3)} + \chi_{ijij}^{(3)} + \chi_{ijji}^{(3)} + \chi_{iiii}^{(3)}). \quad (12)$$

And finally for the (100) crystal face:

$$(\chi_{xyz}^{(2)\text{SEF}})_{(100)} = \begin{pmatrix} 0 & 0 & 0 & 0 & \partial_{15} & 0 \\ 0 & 0 & 0 & \partial_{15} & 0 & 0 \\ \partial_{31} & \partial_{31} & \partial_{33} & 0 & 0 & 0 \end{pmatrix}, \quad (13)$$

where we have

$$\partial_{15} = 3E_z^{\text{surf}} \chi_{iijj}^{(3)},$$

$$\partial_{31} = 3E_z^{\text{surf}} \chi_{ijji}^{(3)},$$

$$\partial_{33} = 3E_z^{\text{surf}} \chi_{iiii}^{(3)}. \quad (14)$$

At this point we note that the form of the tensors in Eqs. (9), (11), and (13) are identical to the tensors representing a pure surface nonlinear optical response for cubic materials.[24] The expected dependence of SH or THz radiation on azimuthal angle is found to be functionally identical to that listed in the paper by Sipe *et al.*[24] Following the above derivation for the bulk fields, we apply the transformation matrix to the effective susceptibility, and evaluate the nonlinear polarization. With this, the radiated fields are found in exactly the same way as for the bulk. The results are listed in Table II.

The coefficients f_s, f_c, t_s, t_p, A_s, A_p, F_s, and F_c in Table II are as defined previously in Table I, and L_{eff} is the effective depth of the medium from which the medium polarization contributes to harmonic radiation. Note that ∂_{ij} of the different crystal orientations are not equivalent and are given by Eqs. (10), (12), and (14) according to the crystal orientation. The angle ϕ is defined in the same way as in Sec. II A.

One finds that the form of the susceptibility tensor for the SEF induced effective second-order nonlinear response is identical to that of an intrinsic surface response.[24] Therefore, in general, crystal rotation measurements alone will not be able to distinguish between these two responses.

III. EXPERIMENT

The experimental setup for investigating the THz emission from the InAs samples is similar to that used in Ref.14. A regeneratively amplified Ti:sapphire laser system (Spectra Physics Hurricane) is used as a pump source, operating at a center wavelength of 800 nm, at 1 kHz repetition rate, with a maximum pulse energy of 750 μJ and a pulse width of 120 fs (Gaussian full width at half maximum). The beam is split into pump (92%) and probe (4%) beams using a wedged window. The probe pulse is delayed with respect to the pump using a scanning optical delay line. A variable attenuator ($\lambda/2$ plate and polarizer) is used in the pump beam to vary the fluence. The THz radiation from the surface of the sample oriented at 45° angle of incidence is collected in the specular direction and imaged onto the ZnTe detector using four F/2 parabolic mirrors. A 1 mm thick ZnTe (110) electro-optic crystal is used as detector or analyzer, which can be oriented either for sensitivity to *p*-polarized THz emission,[29] or to the *s*-polarized THz emission. The InAs samples were rotated about their surface normals.

The InAs samples were mechanically polished, nominally undoped, *n*-type single crystals of 0.5 mm thickness. The InAs (111), (110), and (100) samples had intrinsic carrier concentrations of approximately 3×10^{16} cm^{-3}, 1.9×10^{16} cm^{-3}, and 2.8×10^{16} cm^{-3}, respectively. The carrier mobilities for the InAs (111), (110), and (100) samples were approximately 20 000 cm^2/V s, 22 000 cm^2/V s, and 19 000 cm^2/V s, respectively.

Optical second-harmonic generation (SHG) from the InAs samples was also investigated. The same optical pump source was used, and the setup is similar to that used in Ref. 30. The Ti:sapphire pump laser beam was passed through a polarizer to select *p*-polarized pump and was incident at 45° on the InAs samples. The pump fluence was adjusted to approximately 1 mJ/cm^2 incident on the sample surfaces. A low pass filter was used to block the second harmonic leakage from the laser system prior to striking the sample surfaces. The reflected SH radiation at 400 nm wavelength was collected using a 7.5 cm focal length lens and passed through a short-pass filter to block the fundamental beam. A UV polarizer was used to pass only the *p*-polarized or *s*-polarized second harmonic radiation at 400 nm to a Hamamatsu R7518 photomultiplier tube, which was in turn blocked by a 400 nm interference filter to remove any further leakage of the 800 nm fundamental beam. The InAs samples were rotated about their surface normal.

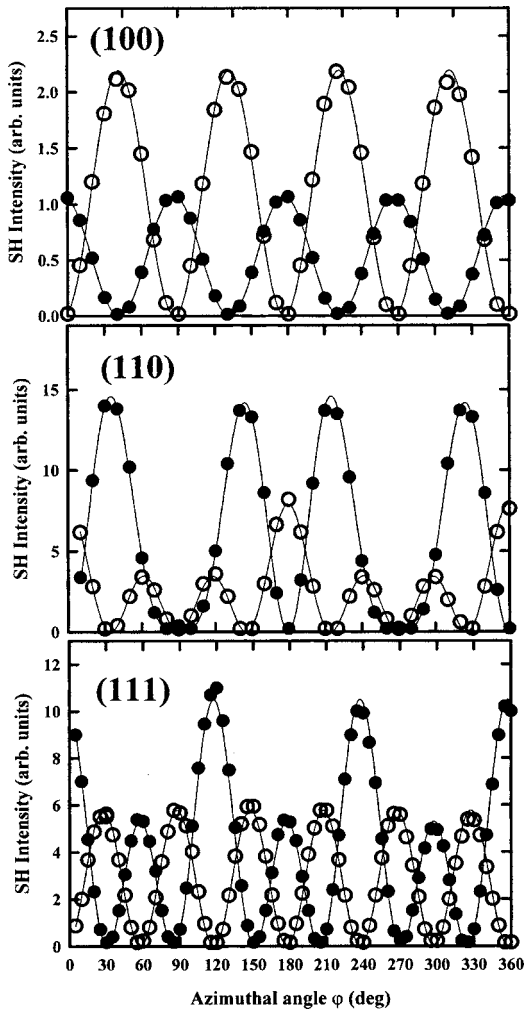

FIG. 2. Azimuthal dependencies of SHG from (100), (110), and (111) faces of *n*-InAs crystals at approximately 1 mJ/cm^2 excitation fluence for *p*-polarized pump radiation. The solid curves represent fits to the data expected for the bulk electric-dipole contribution using the results in Table I. Filled circles represent *p*-polarized SH intensity, and open circles represent *s*-polarized SH intensity. The azimuthal angle is defined as the angle that the projection of the pump beam in the surface plane of the crystal ($\hat{k}$ in Fig. 1) makes with the $[01\bar{1}]$, $[1\bar{1}0]$, and $[\bar{2}11]$ crystal axes for the (100), (110), and (111) crystal faces, respectively. The plots are shown in the same scale.

IV. SECOND-HARMONIC GENERATION

We begin first with results for the SH radiation from the three crystal faces of InAs. The samples are rotated about their surface normal, and the SH intensities are measured as a function of the azimuthal angle ϕ. The results are shown in Fig. 2.

Note that the SH intensity as a function of the azimuthal angle ϕ is described very well by the solid curves in Fig. 2, which are fits to the data based on the appropriate azimuthal dependencies listed in Table I, expected for a bulk electric-dipole contribution to the SH radiation. In general, for crystals that lack inversion symmetry, it is well known that the bulk electric dipole contribution to the SH radiation domi-

TABLE III. Measured and calculated values for ratios of the coefficients in the fitting functions. The ratios are obtained by using the fitting functions and the functional dependence of the radiation on the angle ϕ from Table I.

Expected	Calculated	Measured
$a_3/a_4=(T_p/T_s)(2F_sf_cf_s-F_cf_s^2-(3/4)F_cf_c^2)/[(1/4)f_c^2-f_s^2]$	4.1	4.0±0.2
$b_3/b_4=T_pF_c/T_s$	1.20	1.12±0.04
$a_3/b_3=(2F_sf_cf_s-F_cf_s^2-(3/4)F_cf_c^2)/[(3/4)F_cf_c^2]$	0.97	1.04±0.04
$a_4/b_4=[(1/4)f_c^2-f_s^2]/[(3/4)f_c^2]$	0.29	0.29±0.02
$b_1/b_4=-\sqrt{(2/3)}(4T_pF_c/3T_s)$	1.32	1.28±0.05
$a_2/b_3=-\sqrt{((2/3)}4T_s/(3T_pF_c)$	0.90	0.99±0.04
$b_1/a_4=-\sqrt{(2/3)}(T_p/T_s)(F_cf_c^2)/[(1/4)f_c^2-f_s^2]$	4.6	4.3±0.2
$a_2/a_3=-\sqrt{(2/3)}(T_s/T_p)(f_c^2)/[2F_sf_sf_c-F_cf_s^2-(3/4)F_cf_c^2]$	0.92	0.95±0.03

nates any contribution from the surface terms.[25,31–33]

From the fitting functions, we can verify that the azimuthal dependencies are as expected from Table I, by fitting the resultant angular functions to the data. For the (111) and (110) crystal faces these are $I_{pp}^{\mathrm{SH},111}=[a_1+b_1\cos(3\phi)]^2$, $I_{ps}^{\mathrm{SH},111}=[a_2\sin(3\phi)]^2$, $I_{pp}^{\mathrm{SH},110}=[a_3\sin(\phi)+b_3\sin(3\phi)]^2$, and $I_{ps}^{\mathrm{SH},110}=[a_4\cos(\phi)+b_4\cos(3\phi)]^2$. The coefficients that were obtained by fitting were $a_1=1.5\pm0.1$, $b_1=8.8\pm0.2$, $a_2=7.6\pm0.2$, $a_3=8.0\pm0.2$, $b_3=7.7\pm0.2$, $a_4=2.0\pm0.1$, and $b_4=6.9\pm0.2$. Tabulating some of the coefficient ratios in Table III, we find good agreement with experiment. The values for the index of refraction used in the calculations for the optical pump and second-harmonic wavelengths were $n_{\mathrm{opt}}=3.108+i1.957$ and $n_{2\omega}=3.714+i0.432$, respectively.[34]

The quantities T_s and T_p in Table III are as defined in Ref. 27 and are simply the SH Fresnel transmission coefficients from the InAs into air for the *s*- and *p*-polarized SH, respectively. Similar results are obtained for the (100) crystal face, however a larger deviation from the calculated values was found (20%). This deviation was a result of changing the photomultiplier bias voltage to increase the measured SH signals for the InAs (100).

V. COMPARISON BETWEEN SHG AND THZ RADIATION DUE TO OPTICAL RECTIFICATION

The measured azimuthal dependencies of the radiated THz field are presented next, and compared to the respective SH measurements. In Fig. 3, the THz emission from InAs is plotted with the SH measurements of Sec. IV. Note that as the detection for the terahertz radiation is coherent, the electric field is plotted directly (containing amplitude and phase information), whereas only the intensity of SH is plotted for the SHG data.

First, examining the data for the (100) face in Fig. 3, a large angularly independent contribution to the radiated THz field in the *p*-in *p*-out polarization geometry, and virtually no THz emission in the *p*-in *s*-out polarization geometry have been observed. This could be interpreted as consistent with the THz emission from photocarrier related effects, however, the measured dependence of the THz emission on pump polarization (not shown here) indicate that the magnitude of the carrier-related emission is at most 10–15 % of the total emission.[21] Therefore, the large angularly independent contribution to the *p*-polarized THz field is due to the angularly independent term in Table II.[21] Similarly the lack of a significant *s*-polarized THz emission is also consistent with the expected surface electric-field-induced response listed in Table II.

Possibly the most clear example of the dominance of the effective far-infrared surface response of the InAs is the azimuthal dependence of the THz radiation from the (110) crystal face shown in Fig. 3. Comparing the corresponding expressions from Tables I and II, it is clear that the functional behavior between the effective surface electric-field-induced response and the bulk response will be different. Indeed, examining the THz emission, it is evident that the emission is dominated by surface electric-field-induced optical rectification. The respective solid curves in Fig. 3 are fits to the data based on the expectation that the effective surface electric-field-induced nonlinearity produces the THz output (see Table II). Clearly, the fits are not perfect. This discrepancy is explained by the fact that there exists a contribution to the radiated THz field from bulk optical rectification on the order of 20%.[21] The bulk contribution modulates the angular dependence as the surface and bulk nonlinearity have a different functional dependence on the azimuthal angle.[26]

Therefore the conclusion is that while the bulk nonlinear optical response of the InAs is responsible for the SH radiation, it is the effective surface electric-field-induced nonlinear response of the InAs that is primarily responsible for the emission of THz radiation.

For completeness, the THz emission from InAs (111) is also compared to the SH emission in Fig. 3. The azimuthal dependencies are the same for terahertz and SHG. That is, the threefold rotational symmetry, with an angular shift between the *p*-*p* and *p*-*s* polarization geometries, is exactly the same for terahertz and SHG measurements. This is to be expected since the functional behavior of the surface and bulk contributions is the same (see Tables I and II). Therefore crystal rotation measurements alone cannot distinguish between bulk and surface contributions for radiation from the (111) crystal face.

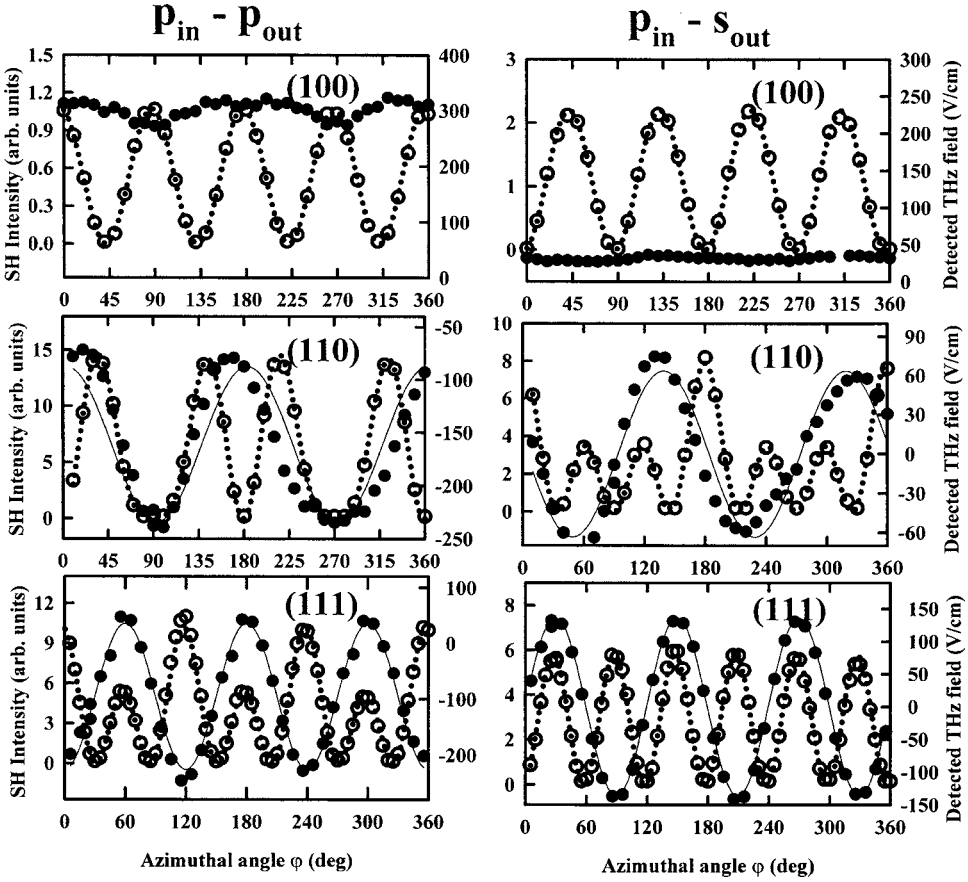

FIG. 3. Comparison of terahertz to SH emission for *p-p* and *p-s* polarization combinations, respectively. Filled circles represent THz emission (scale on right axis), and open circles represent SH intensity (scale on left axis). The solid curves are fits to the THz data based on the expectation of surface electric-field induced optical rectification (Table II), and the dotted curves are fits to the SH intensity based on the expectation of bulk dipole second-order response (Table I). In both measurements, the data is taken at a fluence of $\sim 1\ \mathrm{mJ/cm^2}$. The azimuthal angle is defined as the angle that the projection of the pump beam in the surface plane of the crystal ($\hat{k}$ in Fig. 1) makes with the $[01\bar{1}]$, $[1\bar{1}0]$, and $[\bar{2}11]$ crystal axes for the (100), (110), and (111) crystal faces, respectively.

VI. DISCUSSION

From the present results, the major part of the THz emission from the InAs surfaces is consistent with an effective surface electric-field-induced nonlinearity, whereas the SH emission results from the bulk electric dipole nonlinearity. Since optical rectification and second-harmonic generation are complimentary processes, it may seem strange that they are not governed by the same process in the present study. Based on recent work,[35] it seems likely that the THz emission results from surface-field induced optical rectification rather than a pure surface response. This seems likely as a pure surface response with the symmetry demonstrated in the present report, would result from at most a few monolayers near the surface.[24] In the present case the surface is covered with a native oxide layer, and the samples are single-crystal wafers that were mechanically polished, such a high quality surface is likely not present. Nonetheless, the azimuthal dependence of the radiation in the far-infrared due to optical rectification agrees with an effective surface response due to the combined mechanisms.

The two most important observations made in the present paper are examined next. First, the fact that the SH emission is dominated by bulk electric dipole radiation, whereas the THz emission results primarily from surface electric-field-induced optical rectification. Second, at high excitation fluences, the emission of THz radiation from other semiconductors, such as InP, show a strong bulk contribution to the radiated field.[19] So why is the situation different for THz emission from InAs?

We begin by noting that that there is expected to be a surface field at the mechanically polished, oxidized *n*-InAs surfaces used in the present study as found by Raman scattering in other studies.[36] Given the narrow band gap of InAs, it seems unlikely that there is a several order of magnitude larger surface electric field within InAs as compared to InP, which would be required to explain such a dominant contribution from surface electric-field-induced optical rectification reported here. Therefore, the strong emission due to surface electric-field-induced optical rectification is more likely a result of a strong third-order susceptibility. However, if there exists a strong third-order susceptibility, there must also exist a strong frequency dependence in it as electric-field induced second-harmonic generation is not observed to be dominant from InAs.

A strong third-order susceptibility in the narrow band-gap III-V semiconductors (InAs and InSb) is expected relative to the larger band-gap semiconductors (InP, GaAs etc), based on the theoretical calculations by Ching and Huang.[37] Third-order susceptibilities in the narrow band-gap III-V semiconductors are predicted to be several orders of magnitude larger than in the larger band-gap semiconductors.[37] Moreover, free-carrier contributions to $\chi^{(3)}$ dominate in InAs, whereas the valence-electron contribution tends to dominate in GaAs, for example.[38] Jha and Bloembergen[39] showed that the carrier contribution is expected to scale as $\chi^{(3)}(\omega_4;\omega_1,\omega_2,\omega_3) \propto 1/\omega_1\omega_2\omega_3\omega_4$. This is sufficient to explain the results obtained in the present paper. That is, the far-infrared response of the third-order susceptibility is significantly larger than the response at the second-harmonic frequency. Therefore, one

would expect a much weaker surface electric-field-induced SH intensity in comparison to the electric-field-induced optical rectification signals due to the dispersion in the free-carrier contribution to the susceptibility. Moreover, the third-order susceptibility in InAs is expected to exhibit resonances in the far-infrared due to LO phonon scattering at room temperatures.[40]

Assuming the THz emission is mostly a result of surface electric-field-induced optical rectification, we have sufficient information with the fitting functions and the results in Table II, that we can calculate the ratio of the tensor elements: $\chi^{(3)}_{ijij}/\chi^{(3)}_{iiii}$ for the (110) and (111) crystal faces. This cannot be done for the (100) crystal face as there is only 1 equation in three unknowns (surface-field, two independent tensor elements). An exact determination of the tensor elements, while possible, is complicated by lack of knowledge of the magnitude of the surface field and the fact that the emission is saturated at these high fluences.[21] It should also be noted that the ratio $\chi^{(3)}_{ijij}/\chi^{(3)}_{iiii}$ is the measured ratio in saturation. Using the fitting functions to the data for the (110) and (111) crystal faces: $E_{pp}^{\mathrm{THz},111}=a_1+b_1\cos(3\phi)$, $E_{ps}^{\mathrm{THz},111}=b_2\sin(3\phi)$, $E_{pp}^{\mathrm{THz},110}=a_3+b_3\cos(2\phi)$, and $E_{ps}^{\mathrm{THz},110}=b_4\sin(2\phi)$. The measured values were $a_1=-95\pm7$, $b_1=-130\pm11$, $b_2=137\pm8$, $a_3=-160\pm14$, $b_3=-73\pm18$, and $b_4=-63\pm13$ in V/cm. Given the calculated values for the coefficients a_i and b_i listed in Table II, the extracted ratio $\chi^{(3)}_{ijij}/\chi^{(3)}_{iiii}$ is found to be 0.30 ± 0.03 for the (111) crystal face and 0.26 ± 0.06 for the (110) crystal face. Note that the ratio b_1/b_2 is independent of the surface field and the magnitude of the susceptibility tensor elements. It is calculated to be -1.0 in comparison to the measured value of -1.0 ± 0.1, which agrees very well. The index of refraction used for this calculation are $n_{\mathrm{opt}}=3.714+i0.432$ and $n_{\mathrm{FIR}}=3.868+i0.0039$ at 1.5 eV and 0.01 eV, respectively.[34]

The value of $\chi^{(3)}_{ijij}/\chi^{(3)}_{iiii}\sim0.3$ is in the correct range for III-V semiconductors, but about a factor of three larger than calculated by Ching.[37] This is possibly due to the fact that the data is taken in a saturated regime.

VII. CONCLUSION

The dominant part of the emission of THz radiation from InAs surfaces at high excitation fluences ($1-2$ mJ/cm^2) has been shown to be consistent with surface electric-field-induced optical rectification, whereas second-harmonic emission under the same excitation conditions results from the bulk dipole nonlinearity. Surface electric-field-induced optical rectification is shown to have the same symmetry behavior under crystal rotation that is expected for an intrinsic surface nonlinear response, making it impossible to distinguish between the two processes in the present investigation. However, the intrinsic surface nonlinear response is not expected to dominate the emission of terahertz radiation for the present case as the samples used were mechanically polished and had a native oxide layer. The observation of different processes governing the emission of radiation by the related phenomena of optical rectification and optical second-harmonic generation are attributed to the large third-order susceptibility of InAs at low frequencies compared to higher frequencies. A ratio of $\chi^{(3)}_{ijij}/\chi^{(3)}_{iiii}\sim0.30\pm0.03$ for InAs at low frequencies was calculated based on the experimental data, assuming the emission results from surface electric-field-induced optical rectification. Further measurements at different irradiation intensities would be required to determine how the observed results scale with irradiation fluence.

ACKNOWLEDGMENTS

Financial support provided by MPB Technologies, Inc. and NSERC of Canada is gratefully acknowledged. One of the authors, M.R., acknowledges partial financial support from iCORE.

[1] D. Mittleman, R. Jacobsen, and M. Nuss, IEEE J. Sel. Top. Quantum Electron. **2**, 679 (1996).
[2] D. M. Mittleman, M. Gupta, R. Neelamani, R. G. Baraniuk, J. V. Rudd, and M. Koch, Appl. Phys. B: Lasers Opt. **68**, 1085 (1999).
[3] X.-C. Zhang, Phys. Med. Biol. **47**, 3667 (2002).
[4] K. Kawase, Y. Ogawa, Y. Watanabe, and H. Inoue, Opt. Express **11**, 2549 (2003).
[5] A. Fitzgerald, E. Berry, N. Zinovev, G. Walker, M. Smith, and J. Chamberlain, Phys. Med. Biol. **47**, R67 (2002).
[6] X.-C. Zhang and D. H. Auston, J. Appl. Phys. **71**, 326 (1992).
[7] D. H. Auston, K. P. Cheung, and P. R. Smith, Appl. Phys. Lett. **45**, 284 (1984).
[8] B. B. Hu, X.-C. Zhang, D. H. Auston, and P. R. Smith, Appl. Phys. Lett. **56**, 506 (1990).
[9] L. Xu, X.-C. Zhang, and D. H. Auston, Appl. Phys. Lett. **61**, 1784 (1992).
[10] N. Sarukura, H. Ohtake, S. Izumida, and Z. Liu, J. Appl. Phys. **84**, 654 (1998).
[11] C. Weiss, R. Wallenstein, and R. Beigang, Appl. Phys. Lett. **77**, 4160 (2000).
[12] R. McLaughlin, A. Corchia, M. B. Johnston, Q. Chen, C. M. Ciesla, D. D. Arnone, G. A. C. Jones, E. H. Linfield, A. G. Davies, and M. Pepper, Appl. Phys. Lett. **76**, 2038 (2000).
[13] J. N. Heyman, P. Neocleous, D. Hebert, P. A. Crowell, T. Muller, and K. Unterrainer, Phys. Rev. B **64**, 085202 (2001).
[14] M. Reid and R. Fedosejevs, Appl. Opt. **44**, 149 (2005).
[15] M. Nakajima, M. Hangyo, M. Ohta, and H. Miyazaki, Phys. Rev. B **67**, 195308 (2003).
[16] T. Dekorsy, H. Auer, H. J. Bakker, H. G. Roskos, and H. Kurz, Phys. Rev. B **53**, 4005 (1996).
[17] S. L. Chuang, S. Schmitt-Rink, B. I. Greene, P. N. Saeta, and A. F. J. Levi, Phys. Rev. Lett. **68**, 102 (1992).
[18] D. You, R. R. Jones, P. H. Bucksbaum, and D. R. Dykaar, J. Opt. Soc. Am. B **11**, 486 (1994).
[19] P. N. Saeta, B. I. Greene, and S. L. Chuang, Appl. Phys. Lett. **63**, 3482 (1993).
[20] M. Nakajima, Y. Oda, and T. Suemoto, Appl. Phys. Lett. **85**,

2694 (2004).
[21] M. Reid and R. Fedosejevs, Appl. Phys. Lett. **86**, 011904 (2005).
[22] R. W. Boyd, *Nonlinear Optics*, 2nd ed. (Academic, San Diego, 2003).
[23] T. A. Germer, K. W. Kolasinski, J. C. Stephenson, and L. J. Richter, Phys. Rev. B **55**, 10694 (1997).
[24] J. E. Sipe, D. J. Moss, and H. M. van Driel, Phys. Rev. B **35**, 1129 (1987).
[25] Y. R. Shen, Appl. Phys. B: Lasers Opt. **68**, 295 (1999).
[26] M. Reid and R. Fedosejevs, Proc. SPIE **5577**, 659–669 (2004).
[27] W. Hübner, K. H. Bennemann, and K. Böhmer, Phys. Rev. B **50**, 17597 (1994).
[28] P. N. Butcher and D. Cotter, *The Elements of Nonlinear Optics*, 1st ed. (Cambridge University Press, Cambridge, England, 1990).
[29] P. C. M. Planken, H.-K. Nienhuys, H. J. Bakker, and T. Wenckebach, J. Opt. Soc. Am. B **18**, 313 (2001).
[30] M. Reid, I. V. Cravetchi, R. Fedosejevs, I. M. Tiginyanu, L. Sirbu, and R. W. Boyd, Phys. Rev. B **71**, 081306(R) (2005).
[31] T. Stehlin, M. Feller, P. Guyot-Sionnest, and Y. Shen, Opt. Lett. **13**, 389 (1988).
[32] N. Bloembergen, Appl. Phys. B: Lasers Opt. **68**, 289 (1999).
[33] J. F. McGilp, J. Phys. D **29**, 1812 (1996).
[34] S. Adachi, *Optical Constants of Crystalline and Amorphous Semiconductors*, 1st ed. (Kluwer Academic Publishers, Boston, 1999).
[35] R. Adomavicius, A. Urbanowicz, G. Molis, A. Krotkus, and E. Satkovskis, Appl. Phys. Lett. **85**, 2463 (2004).
[36] S. Buchner, L. Y. Ching, and E. Burstein, Phys. Rev. B **14**, 4459 (1976).
[37] W. Y. Ching and M. Z. Huang, Phys. Rev. B **47**, 9479 (1993).
[38] J. J. Wynne, Phys. Rev. **178**, 1295 (1969).
[39] S. S. Jha and N. Bloembergen, Phys. Rev. **171**, 891 (1968).
[40] A. Mayer and F. Keilmann, Phys. Rev. B **33**, 6962 (1986).